Half Layer By Half Layer Growth of a Blue Phosphorene Monolayer on a GaN(001) Substrate

Jiang Zeng,[1,2] Ping Cui,[1,*] and Zhenyu Zhang[1,†]
[1]*International Center for Quantum Design of Functional Materials (ICQD), Hefei National Laboratory for Physical Sciences at Microscale, and Synergetic Innovation Center of Quantum Information and Quantum Physics, University of Science and Technology of China, Hefei, Anhui 230026, China*
[2]*Beijing Computational Science Research Center, Beijing 100094, China*
(Received 4 June 2016; revised manuscript received 5 December 2016; published 27 January 2017)

Black phosphorene (BlackP), consisting of a vertically corrugated yet single layer of phosphorus atoms, is a latest member of the expanding two-dimensional (2D) materials family with high carrier mobility and immense application potentials. Blue phosphorene (BlueP), an allotrope of BlackP with appealing properties of its own, consists of a more flatly arranged layer of phosphorus atoms. To date, direct growth of either BlackP or BlueP remains a daunting challenge. Using first-principles approaches, here we establish a novel kinetic pathway for fabricating BlueP via epitaxial growth. Our systematic energetic studies reveal that both BlackP and BlueP monolayers can be readily stabilized on Cu(111), Au(111), and GaN(001) substrates. The semiconducting GaN(001) is further shown to be superior for fabricating BlueP, through an intriguing half-layer-by-half-layer (HLBHL) growth mechanism. Within this scheme, the GaN(001) surface is first preferentially covered by a half layer of phosphorus adatoms, followed by the addition of the other half. Once formed, such a BlueP monolayer is thermodynamically stable, as tested using *ab initio* molecular dynamics simulations. The HLBHL growth mechanism discovered here may enable mass production of high-quality BlueP, and could also be instrumental in achieving epitaxial growth of BlackP and other 2D materials.

DOI: 10.1103/PhysRevLett.118.046101

Since the discovery of graphene by mechanical exfoliation in 2004 [1], the synthesis and properties of two-dimensional (2D) or layered materials have been serving as a major drive in condensed matter physics and interdisciplinary sciences. Each new member in the family, such as silicene [2–4], phosphorene [5,6], borophene [7,8], hexagonal boron nitride (*h*BN) [9], transition metal dichalcogenides (TMDs) [10], and even the strong topological insulators [11,12], may invoke a unique mechanism in its fabrication [13], and possess its characteristic properties. Different members of the family also share clear commonalities; for example, the interlayer coupling in most of these materials is relatively weak, typically of the van der Waals (vdW) nature [14]. A more comprehensive understanding of a given member should be instrumental in gaining a better access to the whole 2D materials family.

As a latest member of the 2D materials family, black phosphorene (BlackP) consists of a vertically corrugated yet single layer of phosphorus (P) atoms. As an allotrope of BlackP, blue phosphorene (BlueP) was also predicted to exist in the single layer form [15,16], but with more flatly arranged P atoms. Both systems have been predicted to exhibit exceptionally high carrier mobilities [17,18], with the high mobility of BlackP already experimentally confirmed in the few-layer or monolayer regime using exfoliated samples [5,6]. For future device applications, it is highly desirable to develop efficient fabrication methods for mass production of high-quality phosphorene, such as via epitaxial growth on a proper catalytic substrate. To date, direct growth of high-quality single-layered BlackP or BlueP remains a daunting challenge [19–21].

In this Letter, we use density functional theory (DFT) calculations to explore whether there exists one or more catalytic substrates that can readily facilitate epitaxial growth of monolayered BlackP or BlueP. Our comparative studies of phosphorene growth on different representative surfaces show that BlackP and BlueP can be readily stabilized on Cu(111), Au(111), and GaN(001) substrates. Furthermore, our systematic kinetic studies identify the semiconducting GaN(001) as the substrate of choice for growing BlueP, via a novel and intriguing half-layer-by-half-layer (HLBHL) mechanism. Within this scheme, the surface is first preferentially covered by a half layer (HL) of P adatoms, followed by the addition of the other half, thereby completing a full monolayer (ML) of BlueP. Once formed, such a BlueP ML is thermodynamically stable, as tested using finite-temperature *ab initio* molecular dynamics (AIMD) simulations. The underlying reasons for the HLBHL mode on GaN(001) are attributable to the minimal lattice mismatch in the system, and the naturally strong chemical affinity between the P and substrate atoms. The HLBHL growth mechanism discovered here not only may

enable mass production of high-quality BlueP, but could also be instrumental in achieving epitaxial growth of BlackP and other 2D materials.

Our DFT calculations were carried out using the Vienna *ab initio* simulation package (VASP) [22], where the projector augmented wave (PAW) method [23,24] was adopted, and the generalized gradient approximation (GGA) in the framework of Perdew-Burke-Ernzerhof (PBE) [25] was chosen for the exchange-correlation interaction. Here, we note that different vdW schemes may predict binding energies that scatter by as much as a factor of 2 for a specific test system [26], and there is no *a priori* knowledge about which vdW scheme is more accurate for a given system. In the present study, we consider three different and widely adopted vdW schemes: a specific semiempirical scheme (DFT-D2) [27], the Tkatchenko-Scheffler (DFT-TS) method [28], and a nonlocal correlation functional used to treat the entire range of dispersion interactions in a seamless fashion (vdW-DF2) [29]. The resulting energetic and kinetic quantities are mutually compared to gain a better assurance of the validity of the central findings. The positions of the atoms were obtained by structural optimization until the forces on each atom are smaller than 0.02 eV/Å. A vacuum layer larger than 15 Å is used to avoid possible effects of image supercells. A plane-wave basis was set with a kinetic energy cutoff of 500 eV, and the Brillouin zone was sampled by a $15 \times 15 \times 1$ or $3 \times 15 \times 1$ k mesh, depending on the supercell size. A canonical ensemble was adopted for the AIMD simulations using the algorithm of Nosé [30], with the time step of 2 fs. For the transition state calculations, the climbing-image nudged elastic band (cNEB) method was used to find saddle points and minimum energy paths [31,32].

In previous studies of epitaxial growth of 2D materials such as graphene, silicene, and borophene, catalytic metal substrates have been commonly adopted [2–4,7,8,33]. Certain compound semiconducting or insulating substrates have also been exploited for epitaxial growth of graphene [34] and TMD materials [35]. Whereas metal substrates are typically more effective in catalyzing fast growth [2,7,36], 2D materials grown on semiconducting substrates have the natural advantage of offering richer device potentials without post-growth sample transfer [37].

In the present study, we broadly consider both metal and semiconductor substrates, by first downselecting the candidate substrates to be those with minimal lattice (or superlattice) mismatches between the substrates and either BlackP or BlueP. For the semiconducting substrates, we also pay special attention to systems that share chemical affinity with P. Following these two generic guidelines, we identify five substrates for closer investigations: Au(111), Cu(111), Ga-terminated GaN(001), As-terminated BAs (001), and P-terminated BP(001), with the latter three in the Wurtzite crystal structure. The detailed structures of the combined overlayer and substrate systems are illustrated in Fig. 1, and the corresponding lattice mismatches along the principal directions of BlackP or BlueP are listed in Table 1. The lattice constants of freestanding BlackP are calculated to be $a_a = 4.53$ and $a_b = 3.31$ Å along the armchair and zigzag direction, respectively; the lattice constant of freestanding BlueP is $a_a = a_b = 3.29$ Å. The maximal lattice mismatch is less than 5% along the armchair direction of BlackP on BAs(001), while the minimal mismatch is less than 1% along the armchair direction of BlackP on GaN(001). In assessing the lattice mismatches, we have used superstructures of 2×3, 1×3, 5×1, 5×1, and 5×1 for BlackP on Au(111), Cu(111), GaN(001), BAs(001), and BP(001), respectively. For BlueP, the corresponding superstructures are $(\sqrt{7} \times \sqrt{7})R19.1°$, $(\sqrt{7} \times \sqrt{7})R19.1°$, 1×1, 1×1, and 1×1. The substrates are modeled with slabs of 4 (for metals) or 6 (for semiconductors) atomic layers, with the lowest layer fixed in their respective bulk positions. The bottom layer of a given semiconducting substrate is also terminated by hydrogen atoms.

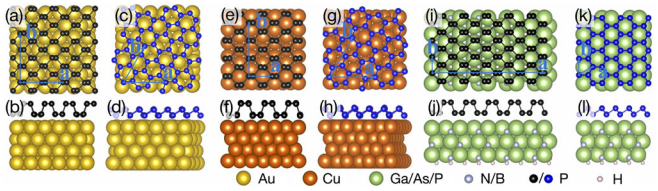

FIG. 1. Top views of the respective BlackP and BlueP on (a) and (c) Au(111), (e) and (g) Cu(111), (i) and (k) any of the three III-V(001) substrates considered. The corresponding side views are given in the lower panels.

To compare the relative stability of BlackP and BlueP on these substrates, we calculate the binding energy per P adatom, defined by $E_b = -(E_t - E_{\text{sub}} - NE_1)/N$. Here, E_t, E_{sub}, and E_1 is the total energy of the combined system, the substrate, and one P atom in freestanding BlackP or

TABLE I. Comparisons of the lattice mismatches and binding energies of BlackP and BlueP on different substrates. Here, a_0 is the lattice constant of the substrate, the different δ values measure the different lattice mismatches for the systems shown in Fig. 1, and E_b measures the corresponding binding energies. The subscript of the binding energy indicates the vdW correction scheme. A negative value of δ indicates that the overlayer is compressively stressed.

		BAs	BP	Cu	Au	GaN
	a_0 (Å)	3.41	3.22	2.56	2.95	3.25
BlackP	δ_a (%)	4.35	−1.65	−1.78	−2.25	−0.60
	δ_b (%)	3.07	−2.86	3.42	2.99	−1.82
	$E_{b\text{-D2}}$ (eV)	0.42	0.56	0.69	0.76	0.71
	$E_{b\text{-TS}}$ (eV)	0.20	0.27	0.37	0.33	0.42
	$E_{b\text{-DF2}}$ (eV)	0.18	0.29	0.30	0.31	0.41
BlueP	δ (%)	3.70	−2.27	2.23	1.75	−1.22
	$E_{b\text{-D2}}$ (eV)	0.49	0.58	0.86	0.88	0.88
	$E_{b\text{-TS}}$ (eV)	0.23	0.32	0.53	0.37	0.49
	$E_{b\text{-DF2}}$ (eV)	0.20	0.31	0.44	0.33	0.45

BlueP, respectively, and N is the total number of P adatoms at a given coverage. We find that the binding energies for BlueP are systematically larger than BlackP on all the substrates considered for the three vdW corrections, indicating that BlueP is consistently more stable, by 0.02–0.17 eV per P atom. This important finding is in qualitative contrast with the results of freestanding BlackP and BlueP, with the former exhibiting a slightly higher cohesive energy per atom (2 meV [16]). We tentatively attribute the reversal of the relative stability to the flatter nature of BlueP, which in turn results in stronger binding between the overlayer and substrate.

Table I shows that the binding energies of BlackP and BlueP MLs on GaN(001), Au(111), and Cu(111) are the largest among the five substrates considered, suggesting that such phosphorene MLs, once formed, are likely to be the most stable structures as well. The binding energies (0.30–0.88 eV) of BlueP and BlackP on the metal substrates are much larger than those of graphene [38,39], but less than those of silicene. For example, the binding energy of graphene on Au(111) is 0.12 eV [39]; in contrast, that of silicene on Ag(111) calculated in this work for comparison is 1.21 eV (with the DFT-D2 correction included), making it extremely difficult to transfer silicene from the metal substrate. BlackP and BlueP grown on metal substrates with intermediate binding energies may encounter similar transferring difficulties. Therefore, among the three promising substrates, the growth of phosphorene MLs on the semiconducting GaN(001) should be the most desirable for various potential device applications. For this very reason, we focus our attention onto GaN(001) in the rest of presentations.

To test whether such MLs on GaN(001) are indeed thermodynamically stable or not, we have performed AIMD simulations at 400 K, below the thermal degradation temperature of about 400 °C for few-layer BlackP [21,40]. In these simulations, we have doubled the supercell size shown in Fig. 1(i) along the zigzag direction for BlackP, and increased the supercell size shown in Fig. 1(k) by (3×3) times for BlueP, to allow the systems to be restructured freely at the given temperature. The results are contrasted in Fig. 2, showing that the BlackP overlayer is drastically distorted at the end of 1 ps AIMD simulations, while the BlueP overlayer essentially preserves its ordered structure even after 50 ps AIMD simulations. Based on these results, we rule out the possibility of growing thermodynamically stable BlackP on GaN(001), while a BlueP overlayer is highly probable to be readily fabricated.

Next we investigate the detailed atomistic processes involved in P adsorption on GaN(001), with the objective of revealing the preferred kinetic pathway towards epitaxial growth of BlueP. We first confirm that a P adatom on GaN(001) is sufficiently mobile, with an activation energy of 0.62 eV [see Fig. 3(a)]. Intriguingly, we find that two P adatoms do not prefer to dimerize; instead, they prefer to stay apart, as also indicated by the adsorption

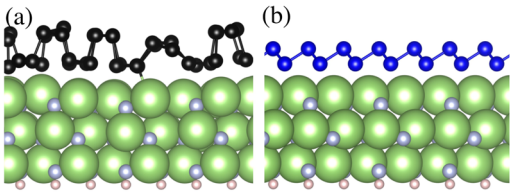

FIG. 2. Contrasting thermodynamic stabilities of (a) BlackP and (b) BlueP on GaN(001) after 1 ps and 50 ps AIMD simulations, respectively. The temperature was identically set at 400 K, and the respective initial configurations are shown in Figs. 1(j) and 1(l).

energy variations for $N = 1$ and 2 shown in Fig. 4(a). The underlying reason is the relatively strong adsorption energy of an isolated P adatom on GaN(001) surface, while the P-P bonding is relatively weak [41]. Furthermore, as shown in Fig. 4(b), at sufficiently low coverages, even three P adatoms prefer to stay apart rather than to form a trimer. Nevertheless, when the GaN(001) surface is populated by sufficiently many P adatoms, nucleation of P islands becomes unavoidable. One such a case is shown in Fig. 4(c), which displays the formation of a P trimer and a lone P adatom when the fractional coverage reaches $\theta = 2/9$, corresponding to a total of four P adatoms within the 3×3 supercell. When the fractional coverage further increases, the energetically preferred state is not given by the formation of a larger island either [13]; instead, more relatively stable trimers are formed, as indicated in the case shown in Fig. 4(d). In

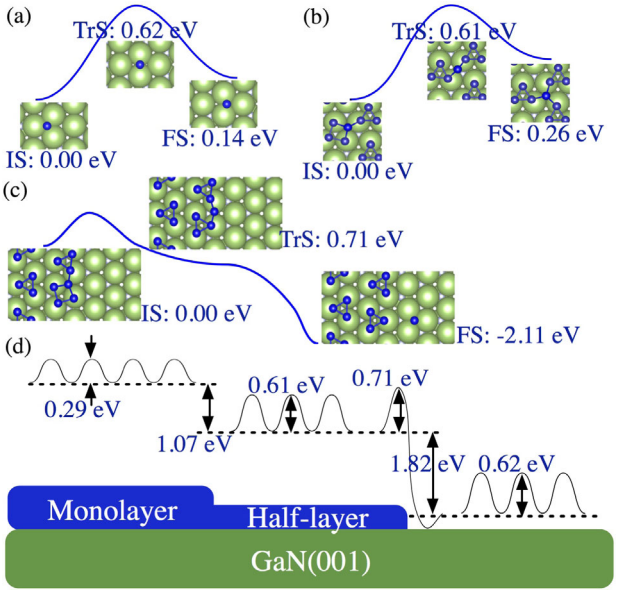

FIG. 3. Diffusion barriers of a P adatom on (a) pure GaN(001) and (b) a P HL-covered GaN(001). (c) Ehrlich-Schwoebel barrier for a P adatom to climb down the step of pure GaN(001) and P HL-covered GaN(001). In (d), all the diffusion barriers for a P adatom are summarized. IS, TrS, and FS represents the initial state, transition state, and final state, respectively.

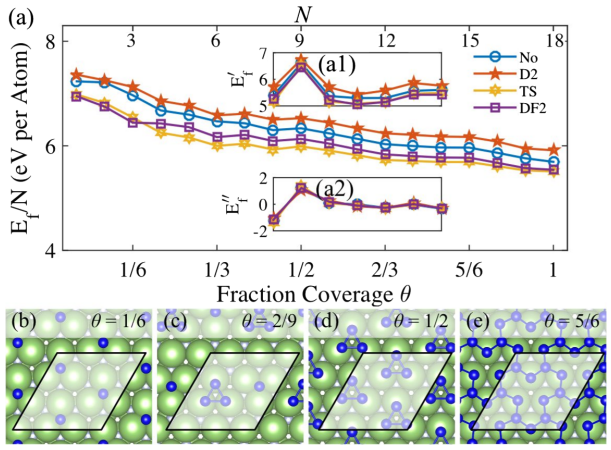

FIG. 4. (a) Formation energy per P adatom E_f/N as a function of the fraction coverage θ on GaN(001), where $E_f = -(E_t - E_{\mathrm{sub}})$. The insets (a1) and (a2) give the first and second difference of the formation energy as a function of the fraction coverage θ, respectively. No, D2, TS, and DF2 denote the data obtained without vdW correction, with DFT-D2, DFT-TS, and vdW-DF2 corrections, respectively. (b)–(e) Representative configurations at different P coverages.

particular, when $\theta = 1/2$ (namely, reaching equivalent one HL of BlueP), the 3×3 supercell is covered by three equally spaced P trimers, whose overall structural configuration yet does not indicate any apparent connection to the eventual BlueP overlayer. We have also explicitly verified that the configuration shown in Fig. 4(d) is much more stable than placing all the nine P adatoms into a partial BlueP overlayer configuration while leaving the other half of the GaN(001) surface unoccupied. When an extra P adatom is added onto such a HL, it can diffuse from one trimer to a neighboring trimer, with a slightly lower activation energy of 0.61 eV [see Figs. 3(b) and 3(d)]. As indicated by the situation shown in Fig. 3(c), such an extra P adatom reaching the upper edge of the trimerized structure prefers to climb down from an edge trimer if the GaN(001) surface has not been fully covered by the P trimers yet. The corresponding barrier is 0.71 eV, revealing a low but positive Ehrlich-Schwoebel barrier [42,43] in this system [see Figs. 3(c) and 3(d)]. The values of the diffusion barriers presented in Fig. 3 are calculated using the DFT-D2 scheme. Overall, because a barrier is given by the energy difference between the initial and transition state, it varies little (≤ 0.1 eV) among the three different vdW schemes.

As an interim summary, we emphasize that so far the growth picture depicted above for the equivalent HL of BlueP is qualitatively different from the traditional nucleation and growth picture. Traditionally, adatoms diffuse to nucleate islands of critical sizes, which further enlarge in subsequent growth, eventually forming monolayered or multilayered films.

Now we go beyond the HL regime, which represents a local maximum in the average formation energy per adatom and a distinct peak in both the first and second difference, defined by $E_f' = E_f(N) - E_f(N-1)$ and $E_f'' = 2E_f(N) - E_f(N+1) - E_f(N-1)$, respectively [Fig. 4(a)]. In particular, E_f'' at $\theta = 1/2$ is distinctively positive, signifying the extra stability of the HL. Earlier we have shown that when a P adatom is deposited on top of an incomplete HL, it can diffuse and climb down. When an extra P adatom is deposited onto a complete HL, it will stay on top of the HL by inducing local structural distortions into the resided P trimer, diffuse around [see Fig. 3(b)], and signify the initial growth of the second HL. We have verified that two P adatoms deposited onto the first HL will also prefer to stay apart rather than to form a dimer, introducing more local structural distortions into the respective resided P trimers. When even more P adatoms are added on top, more energetically close configurations can exist, accompanied by more dramatic distortions into the initially trimerized HL. Here we have also verified that three atop P adatoms will not form a trimer; instead, each one breaks its resided trimer. Importantly, local structures that mimic metastable BlueP can be initialized when the P coverage in the second HL further increases, as illustrated in a representative configuration shown in Fig. 4(e). Crucially, when the total coverage reaches the equivalent ML of BlueP, the energetically most stable configuration is indeed that of the BlueP, as shown in Figs. 1(k) and 1(l).

Putting the above presentations together, we reach the HLBHL epitaxial growth scheme for BlueP on GaN(001).This novel mechanism is further validated by the additional investigation of the adsorption and diffusion of one extra P adatom deposited on top of a BlueP segment. The results are shown in Fig. 3(d), indicating that such an adatom can readily diffuse and climb down to reach the top of the first HL. Therefore, the growth of multilayered BlueP would unlikely take place before the completion of the first ML.

Here we emphasize the significance and novelty of the HLBHL growth mode, whose validity is accompanied by three distinct characteristics: (i) the adatom-substrate bonding is too strong for two isolated adatoms to dimerize; (ii) the overall contour of the average formation energy per adatom decreases with increasing coverage; (iii) the ending structure should have a vertically corrugated configuration within one layer. Such characteristics are shown to be possessed by the BlueP system, and likely to be also shared by other corrugated 2D systems such as silicene. In contrast, typical 3D growth systems do not necessarily possess such characteristics (especially the vertical corrugations within one layer) [44,45]. The underlying reason differentiating 2D and 3D growth systems may be very likely tied to the existence of vdW-type coupling at the interface in the former case, thereby allowing larger degrees of vertical corrugations within one monolayer.

In summary, our comparative total energy calculations have shown that BlackP and BlueP monolayers can be readily stabilized on Cu(111), Au(111), and GaN(001),

with the semiconducting GaN(001) inherently highly preferred among the three for various device applications. Furthermore, our systematic energetic and kinetic studies of P adatoms, clusters, and MLs have revealed a novel HLBHL growth mechanism for fabricating monolayered BlueP on Ga-terminated GaN(001). Once formed, such a BlueP ML is thermodynamically stable, as tested using AIMD simulations at 400 K. The HLBHL growth mechanism discovered here may also be applicable to epitaxial growth of BlackP and other 2D materials.

We thank Dr. Wei Chen for helpful discussions. This work was supported by the National Natural Science Foundation of China (Grants No. 11634011, No. 61434002, No. 11374273, and No. U1530401) and the National Key Basic Research Program of China (Grant No. 2014CB921103). The calculations were performed at the National Supercomputing Center in Shenzhen.

Note added.—After the submission of this Letter, a report on experimental growth of nearly monolayered BlueP on Au(111) has appeared [46], while the growth of high-quality BlueP or BlackP on a semiconducting substrate remains a standing challenge.

*Corresponding author.
cuipg@ustc.edu.cn
†Corresponding author.
zhangzy@ustc.edu.cn

[1] K. S. Novoselov, A. K. Geim, S. V. Morozov, D. Jiang, Y. Zhang, S. V. Dubonos, I. V. Grigorieva, and A. A. Firsov, Science **306**, 666 (2004).
[2] P. Vogt, P. De Padova, C. Quaresima, J. Avila, E. Frantzeskakis, M. C. Asensio, A. Resta, B. Ealet, and G. Le Lay, Phys. Rev. Lett. **108**, 155501 (2012).
[3] B. Feng, Z. Ding, S. Meng, Y. Yao, X. He, P. Cheng, L. Chen, and K. Wu, Nano Lett. **12**, 3507 (2012).
[4] A. Fleurence, R. Friedlein, T. Ozaki, H. Kawai, Y. Wang, and Y. Yamada-Takamura, Phys. Rev. Lett. **108**, 245501 (2012).
[5] L. Li, Y. Yu, G. J. Ye, Q. Ge, X. Ou, H. Wu, D. Feng, X. H. Chen, and Y. Zhang, Nat. Nanotechnol. **9**, 372 (2014).
[6] H. Liu, A. T. Neal, Z. Zhu, Z. Luo, X. Xu, D. Tománek, and P. D. Ye, ACS Nano **8**, 4033 (2014).
[7] A. J. Mannix *et al.*, Science **350**, 1513 (2015).
[8] B. Feng, J. Zhang, Q. Zhong, W. Li, S. Li, H. Li, P. Cheng, S. Meng, L. Chen, and K. Wu, Nat. Chem. **8**, 563 (2016).
[9] L. Song, L. Ci, H. Lu, P. B. Sorokin, C. Jin, J. Ni, A. G. Kvashnin, D. G. Kvashnin, J. Lou, B. I. Yakobson, and P. M. Ajayan, Nano Lett. **10**, 3209 (2010).
[10] Q. H. Wang, K. Kalantar-Zadeh, A. Kis, J. N. Coleman, and M. S. Strano, Nat. Nanotechnol. **7**, 699 (2012).
[11] H. Zhang, C.-X. Liu, X.-L. Qi, X. Dai, Z. Fang, and S.-C. Zhang, Nat. Phys. **5**, 438 (2009).
[12] Y. L. Chen *et al.*, Science **325**, 178 (2009).
[13] Z. Y. Zhang and M. G. Lagally, Science **276**, 377 (1997).
[14] A. K. Geim and I. V. Grigorieva, Nature (London) **499**, 419 (2013).
[15] J. C. Jamieson, Science **139**, 1291 (1963).
[16] Z. Zhu and D. Tománek, Phys. Rev. Lett. **112**, 176802 (2014).
[17] J. Qiao, X. Kong, Z.-X. Hu, F. Yang, and W. Ji, Nat. Commun. **5**, 4475 (2014).
[18] J. Xiao, M. Long, X. Zhang, J. Ouyang, H. Xu, and Y. Gao, Sci. Rep. **5**, 9961 (2015).
[19] Z. Yang, J. Hao, S. Yuan, S. Lin, H. M. Yau, J. Dai, and S. P. Lau, Adv. Mater. **27**, 3748 (2015).
[20] M. Zhao, H. Qian, X. Niu, W. Wang, L. Guan, J. Sha, and Y. Wang, Cryst. Growth Des. **16**, 1096 (2016).
[21] J. Gao, G. Zhang, and Y.-W. Zhang, J. Am. Chem. Soc. **138**, 4763 (2016).
[22] G. Kresse and J. Furthmüller, Phys. Rev. B **54**, 11169 (1996).
[23] P. E. Blöchl, Phys. Rev. B **50**, 17953 (1994).
[24] G. Kresse and D. Joubert, Phys. Rev. B **59**, 1758 (1999).
[25] J. P. Perdew, K. Burke, and M. Ernzerhof, Phys. Rev. Lett. **77**, 3865 (1996).
[26] E. Mostaani, N. D. Drummond, and V. I. Fal'ko, Phys. Rev. Lett. **115**, 115501 (2015).
[27] S. Grimme, J. Comput. Chem. **27**, 1787 (2006).
[28] A. Tkatchenko and M. Scheffler, Phys. Rev. Lett. **102**, 073005 (2009).
[29] K. Lee, E. D. Murray, L. Kong, B. I. Lundqvist, and D. C. Langreth, Phys. Rev. B **82**, 081101 (2010).
[30] S. Nosé, J. Chem. Phys. **81**, 511 (1984).
[31] G. Henkelman, B. P. Uberuaga, and H. Jónsson, J. Chem. Phys. **113**, 9901 (2000).
[32] H. Jónsson, Annu. Rev. Phys. Chem. **51**, 623 (2000).
[33] W. Chen, H. Chen, H. Lan, P. Cui, T. P. Schulze, W. G. Zhu, and Z. Y. Zhang, Phys. Rev. Lett. **109**, 265507 (2012).
[34] W. Yang *et al.*, Nat. Mater. **12**, 792 (2013).
[35] K. Kang, S. Xie, L. Huang, Y. Han, P. Y. Huang, K. F. Mak, C.-J. Kim, D. Muller, and J. Park, Nature (London) **520**, 656 (2015).
[36] L. Liu *et al.*, Proc. Natl. Acad. Sci. U.S.A. **111**, 16670 (2014).
[37] C. R. Dean, A. F. Young, I. Meric, C. Lee, L. Wang, S. Sorgenfrei, K. Watanabe, T. Taniguchi, P. Kim, K. L. Shepard, and J. Hone, Nat. Nanotechnol. **5**, 722 (2010).
[38] M. Vanin, J. J. Mortensen, A. K. Kelkkanen, J. M. Garcia-Lastra, K. S. Thygesen, and K. W. Jacobsen, Phys. Rev. B **81**, 081408(R) (2010).
[39] J. Sławińska, P. Dabrowski, and I. Zasada, Phys. Rev. B **83**, 245429 (2011).
[40] X. Liu, J. D. Wood, K.-S. Chen, E. Cho, and M. C. Hersam, J. Phys. Chem. Lett. **6**, 773 (2015).
[41] H. Chen, W. G. Zhu, and Z. Y. Zhang, Phys. Rev. Lett. **104**, 186101 (2010).
[42] G. Ehrlich and F. G. Hudda, J. Chem. Phys. **44**, 1039 (1966).
[43] R. L. Schwoebel and E. J. Shipsey, J. Appl. Phys. **37**, 3682 (1966).
[44] J. A. Carlisle, T. Miller, and T.-C. Chiang, Phys. Rev. B **47**, 3790 (1993).
[45] H. H. Weitering, J. M. Carpinelli, A. V. Melechko, J. Zhang, M. Bartkowiak, and E. W. Plummer, Science **285**, 2107 (1999).
[46] J. L. Zhang, S. Zhao, C. Han, Z. Wang, S. Zhong, S. Sun, R. Guo, X. Zhou, C. D. Gu, K. D. Yuan, Z. Li, and W. Chen, Nano Lett. **16**, 4903 (2016).